ILASS 2008
Sep. 8-10, 2008, Como Lake, Italy

Paper ID ILASS08-12-1

SPRAY CHARACTERISTICS OF A KEROSENE JET IN CROSS FLOW OF AIR AT ELEVATED PRESSURE

Stefan Freitag, Christoph Hassa

German Aerospace Center (DLR), Institute of Propulsion Technology, Linder Höhe, 51147 Cologne, Germany

ABSTRACT

The goal of the current investigation was to enlarge the existing dataset with penetration and atomization data for three different nozzle diameters. Kerosene was used throughout the tests but nozzle diameter, air velocity, pressure and the momentum flux ratio were varied. Shadowgraphy was employed to measure the liquid penetration and show the general spray characteristics. Droplet diameters, velocity- and fuel flux distributions were measured with a Phase Doppler Anemometer 100 mm downstream of the jet nozzle. In addition to momentum ratio, the jet penetration is also strongly influenced by the nozzle diameter. Concerning the droplet size the dependence on the nozzle diameter was small compared with the influence of air velocity and pressure. A correlation for these cases with a quotient of aerodynamic Weber number We_{aero} and nozzle diameter D greater than 1.2E+06 of surface breakup is given in the following equation:

$$\frac{z}{D} = 1.6 \cdot q^{a} \cdot \ln\left(1 + 3.81 \cdot \frac{x}{D}\right) \qquad \begin{aligned} &q = 3 - 24; \quad We_{aero} / D = 1.2E + 06 - 2.3E + 06; \\ &a = 0.4; \quad x / D = 1.4 - 50 \end{aligned}$$

INTRODUCTION

Injection of liquid fuel in a flow of air with a circular jet is a convenient means for fuel placement in gas turbines, especially if lean combustion is intended in the combustor. Compared to pressure swirl or prefilming air-blast atomizers, a multipoint source that is constituted by an array or a matrix of jets allows distribution of the fuel over a wider range of combustion air. Thus a preliminary step to premixing of fuel and air can be achieved already in the liquid flow path, as the fuel can be transported nearer to the streamline of the combustion air where it should mix as homogenously as possible before entering the flame without having to migrate to his streamline in the combustor. The first challenge associated with multipoint injection is the prevention of overheating of the liquid in the feed line, as fuel coking can lead to partial or ultimately complete blockage of fuel lines and inhomogeneous fuel distribution resulting in hot streaks and unsafe combustor operation. Hence there is a practical limit to the degree of exposition of the point source to the hot gas flow, the number of points and size of the point source which leads to the second challenge of multipoint injection: Knowing how to transport the fuel to the intended streamline. Jets in cross flow present themselves as a potential solution, as they can provide penetration of liquid into the gaseous flow from a position where coking can be prevented. However they also present a further challenge as the jet penetration and atomization in a hot and often swirling stream of gas of high turbulence escapes the computational capacities of numerical models and the predictive capacities of semi-empirical or empirical models for some time to come. Turbulence, heat flux and surface properties interact coupling the penetration and atomization of the jet to the gas phase on a macroscopic and microscopic scale. Unfortunately the cross flow in which the liquid is injected often has high velocity gradients and a slight misplacement of the fuel can result in higher pollutant emission or reduced combustion stability. This is the reason for the growing interest about the behaviour of jets in cross flow at various operating conditions. The absence of means to predict or even measure the mixing from jets in cross flow in fully realistic conditions enforces an investigation strategy with a stepwise increase of realism, starting from injection in uniform flow [1] to injection in swirling flow [2] and ultimately in combustors [3], where correlations can be created only in the first step and CFD calculations with initial conditions for the dispersed phase then have to be used to validate the latter and then ultimately to extrapolate to gas turbine engine conditions.

Previous studies of liquid injection in crossflows include analyses of liquid jets atomized at different conditions. One of the key points of these analyses is the investigation of the jet penetration [5, 7, 8]. In these studies the test conditions, measurements and evaluation methods vary considerably. Chen [5], Wu [7], and Inamura [8] chose very high air flow velocities of up to 140 m/s with atmospheric pressure and a considerable variation of hole diameters, with the usually upper limit of 2 mm. Becker [1] and Bellofiore [4] varied amongst other parameters the static air pressure and temperature while using kerosene as liquid. Shadowgraphs and Mie-Scattering are the standard measurement methods. Exposure times varied between 33 µs [8] and 8 ns [5]. Accordingly averaging over a long exposure time and averaging over many pictures was used in the penetration analysis of the two extreme cases.

The second most interesting point of liquid injection in crossflow is the mean drop size of the global spray. Hussein et al. [10] have investigated the SMD at atmospheric pressure

as a function of numerous parameters, including liquid and nozzle properties. Other, less detailed investigations using real jet engine fuels included a variation of pressure and pointed to surface tension, air density, and air velocity as the main parameters affecting drop sizes of low viscosity liquids such at water or kerosene [9, 11].

EXPERIMENT METHODS

Test Rig and Cell

Tests were conducted in a quartz glass duct of quadratic cross section of 40 by 40 mm depicted in Fig. 1. This test cell is mounted inside the pressure housing so that it is surrounded by a cooling air flow. The pressure housing is equipped with quartz glass pressure windows on both sides and on top. The maximum test conditions are a pressure of 20 bar, an air mass flow of 1.5 m³/ s and a temperature of 850 K. The optically accessible length of the duct is around 150 mm.

The test section is fed with the main air flow, which can be preheated by an electrical air heater with a power input of 520 KW. The cooling air flow is controlled separately to achieve the desired pressure. Both main air and supplementary air leave the pressure housing through a common throttle that acts as sonic nozzle. By selecting one of a number of a different size throttles, the air velocity range at a given temperature in the test cell is preset independently of pressure. The exact value of air velocity is then obtained by fine-tuning of the flow split between main and supplementary air. Both volumetric air flows are measured separately by vortex meters. Air pressure and air temperature are measured at the inlet of the test cell by means of a pressure transducer and a NiCr-Ni thermocouple. The fuel mass flow is measured with a coriolis meter. The temperature of the fuel is measured outside of the pressure
housing by a NiCr-Ni thermocouple. During tests, all variables such as air flows, temperatures and pressures are logged automatically at 3-second intervals on a PC.

The test rig is equipped with two atomizer ports to adopt the nozzle. For the PDA-measurements, the first port and for the shadowgraphs the second port in the downstream direction was used. So the placement and orientation of the shown co-ordinate system is well-defined for PDA-measurements at which the y- coordinate is orthogonal to the x-z-plane in a standard right hand orientation.

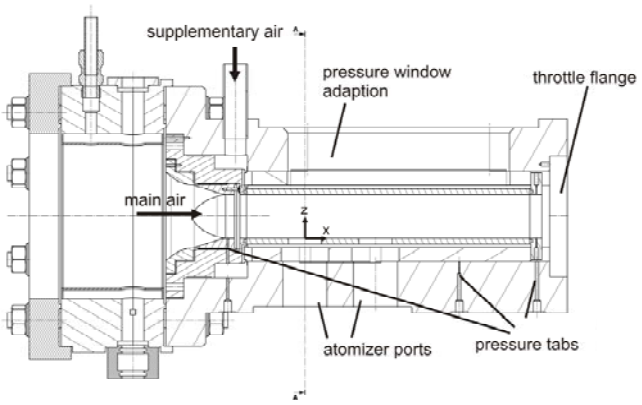

Fig. 1 LP(P) Test Cell

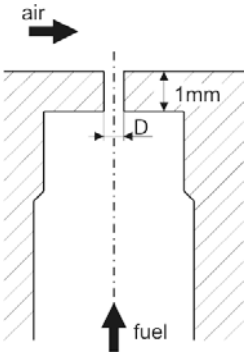

Fig. 2 Schema of nozzle geometry

Three different dimensions of nozzles were employed in the course of this project. In Fig. 2 schematic of the plain jet nozzle is depicted. The inappropriately design of the prechamber concerning fluid mechanics is based on the relevance of technical burner used up as a Pre-ring channels. The three nozzles differ in diameters with D = 0.3, 0.5 and 0.7 mm. Manufacturing consisted of drilling and reaming and was done by the machine shop of the cologne centre of DLR.

Measurements

The investigation of fuel atomization with Shadowgraphs was carried out to analyze the jet penetration and breakup mechanisms and to compare the differences between the test conditions particularly with regard to the influence of the nozzle diameter. The knowledge of these physical phenomena is important for the understanding of the PDA results.

The fuel was illuminated by a flash lamp with a pulse-duration of about 2 µs. On the other side of the test cell, a CCD camera (PCO.1600) with a maximum resolution of 1600x1200 pixels was positioned and triggered by the flash lamp. The time interval (delay time) between the photos was around 100 ms. The camera was positioned such, that the principal axis of its front lens (Nikon 35mm) was in plane with the floor of the glass duct. The intensity of light was varying with distance in axial direction of the glass duct. Therefore, the chosen size of the imaged area was 19 x 13 mm. It was projected on a CCD region of 800 x 601 pixels.

Table 1 Test conditions for shadowgraphs (S) and PDA (P)

p_{air} MPa	u_{air} m/s	q -	We D=0.3mm	We D=0.5mm	We D=0.7mm	
0.4	75	6	352	586	820	S/P
0.2	75	6	176	293	410	S/P
0.6	75	6	527	879	1230	S/P
0.8	75	6	703	1172	1641	S/P
0.4	25	6	39	65	91	S
0.4	50	6	156	260	365	S/P
0.4	100	6	625	1042	1458	S/P
0.4	150	6	1406	2344	3281	P
0.4	75	3	352	586	820	S/P
0.4	75	12	352	586	820	S/P
0.4	75	24	352	586	820	S/P

Table 1 gives an overview of the shadowgraphs and PDA test conditions. The columns 4-6 of the table comprise the aerodynamic Weber numbers to the three nozzle dimensions

correspondingly. The last column marks the measurement method. With 10 different test conditions and 3 different nozzles these are all in all 30 test conditions per measurement method. For the shadowgraphs every test case at least 100 images were taken. A Dantec 2-D PDA system was used for the investigations of droplet size and two components of the velocity of droplets. The power of the several laser beams in the distance of measurement volume was around 20 mW. The interspace between a beam pair on the exit of the transmitting optics amounted to 23 mm. The focal length of the transmitting and of the receiving optics was 310 mm. The resulting measurement volume had a diameter of about 69 μm and a length in the y-direction of 1.9 mm, but was limited in the y-direction by a slit of 100 nm in the receiving optics. The value of the off-axis angle of the receiving optics was 50°.

To anticipate a shadow effect on the aperture of the receiving optics the complete optical set-up was tilted around the principal axis of the transmitting optics by 6.4°. Thus, the whole lens of the receiving optics was always above the bottom of the duct and therefore completely unblocked. As a matter of course the raw data were subjected to a coordinate transformation to obtain the velocities in the x-z coordinate system.

The termination condition was set at 40.000 validated particles for every measurement point. If the 40.000 particles were not recorded within 30 seconds, the measurement was terminated and a lower number of particles down to 50 Hz were stored. Thus the size of a measurement plane with the several measurement points was depended on the data rate and hence from the Fuel Flux. The grid spacing was 2 millimetre for all measurement planes.

For lower distances from the transmitting optics to the glass duct the lower beam of the vertical beam pair was cut off by the bottom of the glass duct and therefore the bottom boundary edge was set by the minimal feasible distance of two millimetres between the bottom of the duct and the measuring volume.

In Table 1 there is an overview of the thirty PDA test conditions. These measuring cases correspond to the conditions of shadowgraphs with the slight difference that instead of an air velocity of u_{air} = 25m/s, an air velocity of uair = 150m/s was measured. This happened under the assumption that the smaller droplets associated with higher air velocity were of higher relevance for the expected combustor operating range.

RESULTS

Shadowgraphs

In Fig. 3 two main mechanisms of jet breakup can be recognized. These are the column breakup on one hand and the surface breakup on the other. Usually, both breakup mechanisms are active, but one is dominant.

As a typical feature of the column breakup mechanism, the emergence and growth of waves on the windward surface of the jet can be observed in the picture on the left-hand side in Fig. 3. According to their occurrence wave troughs emerge giving rise to the formation of ligaments and large drops which subsequently detach from the body of the jet. The

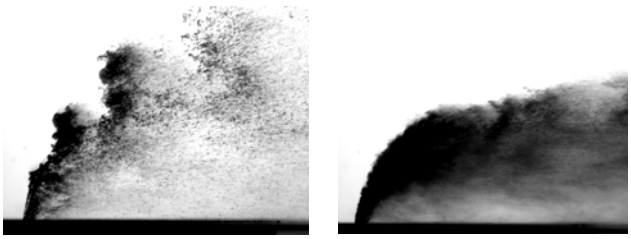

Fig. 3 Breakup mechanisms; left: dominant column breakup; right dominant surface breakup

magnification used is not sufficient to identify the origin of the wave through formation. For different pictures at the same test condition the wavelength of wave troughs are different, there is no apparent regularity.

A characteristic of surface breakup as observed in our parameter range is the continuous breakup alongside the liquid jet column up to the final jet breakup point, as seen on the right-hand side in Fig. 3. The fuel is stripped off the surface of the liquid column by the shearing action of the air flow. Wu et al. [7] described surface breakup as dependent on We and q. They analysed the penetration at very high momentum ratios of up to q = 185 and found surface breakup exclusively on the cylindrical jet before the occurrence of liquid column instabilities.

In the following the instantaneous shadowgraphs are depicted for the different test conditions around the baseline case.

Fig. 4 exhibits the stepwise rise of air velocity. The images present the test cases for D = 0.5 mm and the accompanying test conditions according to the table 1. For the test case u_{air} = 25 m/s the liquid penetration is very high, ligaments and big drops are formed with a length of up to 0.2 mm. The reason for the formation of such big drops is of course the small relative velocity. The increase of the air velocity causes a finer and more even atomization and a gradual shift from the dominance of column breakup to surface breakup. In addition the visible large scale coherent structures and forms disappear with higher velocity.

The stepwise rise of static air pressure in Fig. 5 produces the same trend but in a smaller range. Consequently is to be supposed that both parameters cause a finer and more even atomization.

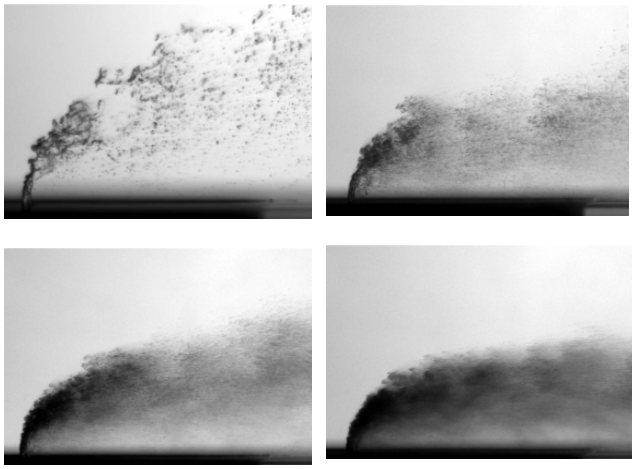

Fig. 4 The effect of air velocity: top left 25 m/s; top right 50 m/s; down left 75 m/s; down right 100 m/s

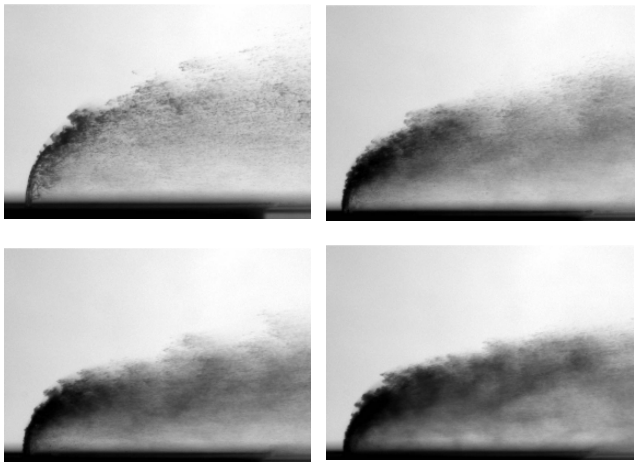

Fig. 5 The effect of air pressure: top left 0.2 MPa; top right 0.4 MPa; down left 0.6 MPa; down right 0.8 MPa

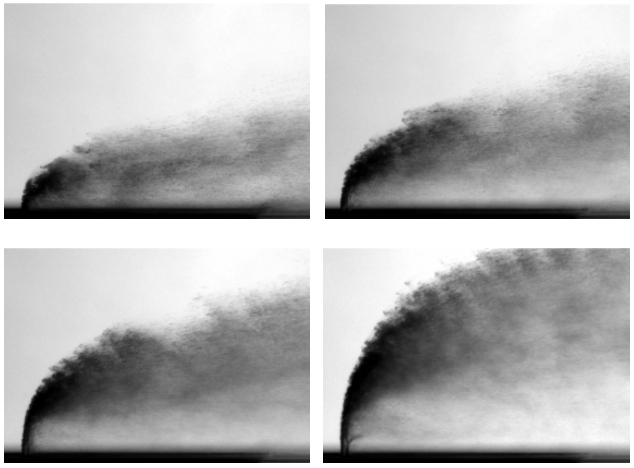

Fig. 6 The effect of momentum flux ratio: top left q = 3; top right q = 6; down left q =12; down right q = 24

The variation to higher values of the momentum flux in Fig. 6 effected a higher jet penetration. A decisive variation of the breakup characteristics cannot be stated.

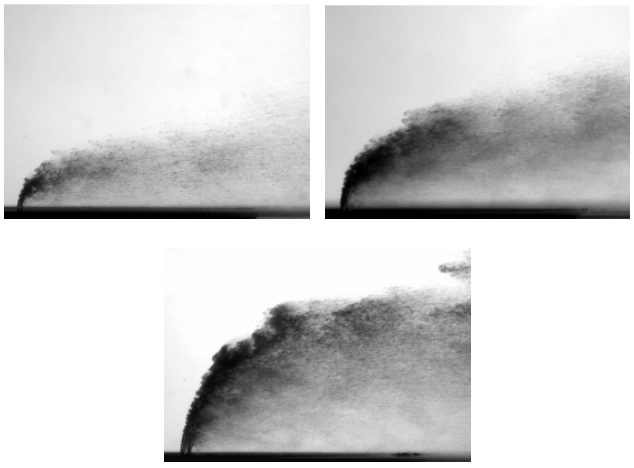

Fig. 7 The effect of hole diameter: top left D = 0.3 mm; top right D = 0.5 mm; down D = 0.7 mm

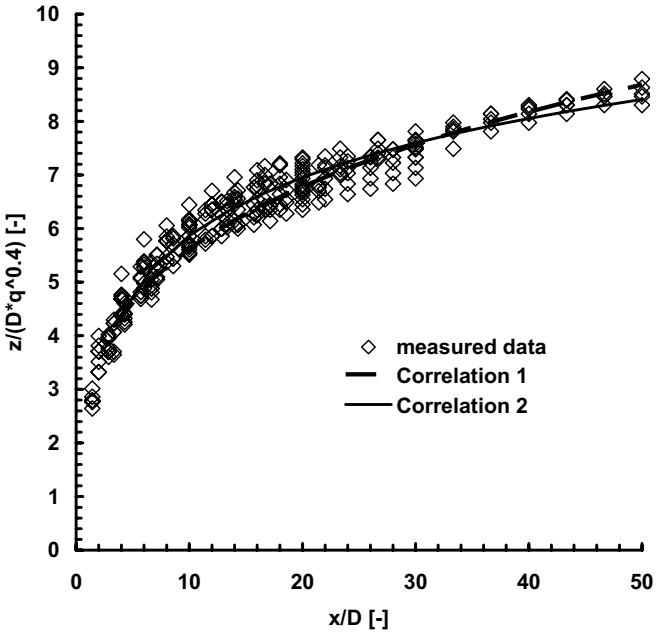

Fig. 8 Correlation of the liquid penetration for dominated surface breakup cases

Fig. 7 shows the influence of the nozzle diameter on the penetration for the same operating condition. It is to be recognized, that jet penetration, which is clearly a function of momentum flux ratio, is also strongly influenced by nozzle diameter.

It is clearly recognizable that column breakup is dominant for mild air conditions, i.e. low dynamic pressure of the air flow, while surface breakup dominates when the dynamic pressure of the airflow is high.

For the case dominated by surface breakup, the shadowgraphs suggest an average liquid penetration with low fluctuations. A correlation for these cases according to the parameters in table 1 with a quotient of aerodynamic Weber number and nozzle diameter We/D greater than 1.17E+06 of surface breakup is illustrated in Fig. 8.

For each value of the abscissa x/D the measured data points indicate the location of the maximum intensity gradient in the vertical direction from the clear background to upper random of fuel. These locations results from an averaging of 100 pictures. Equation (1) describes the Correlation 1 in Fig. 8 with a correlation coefficient of r = 0.97:

$$\frac{z}{D} = 3 \cdot q^{0.4} \cdot \left(\frac{x}{D} \right)^{0.27} \qquad (1)$$

From equation 1 follows that the penetration of a constant volume flow through the fuel nozzle is increased when the jet diameter is reduced. A little better correlation coefficient of r 0.98 is achieved by the correlation 2 cp. Fig. 8 with respect to Eq. (2).

$$\frac{z}{D} = 1.6 \cdot q^{0.4} \cdot \ln\left(1 + 3.81 \cdot \frac{x}{D} \right) \qquad (2)$$

It is interesting to observation the low variations of data points and the correlations and hence the almost sole

dependence of momentum flux ratio q for the test case of surface breakup regimes. The exponent of momentum flux ratio is agreement very well with those in the literature [1, 4, 5, 8] which based on a similar q-interval.

PDA-results

Fig. 9 and Fig. 10 present the PDA data exemplary in the form of contour plots of volumetric fuel flux and SMD in the y-z plane at the location hundred millimetres downstream of the jet nozzle. To compute the volumetric fuel flux from the raw data, an in-house post-processing routine was used [6]. The integrated data resulted for many test cases a different measured mass flux as in set by the fuel flow. Because of this circumstance, for every test case the Fuel Flux was scaled with the associated test case. The distribution of the fuel flux should be self explanatory and are nearly circular. The centre of these circle respectively the maximum values of fuel flux is another representation of the jet penetration. For the individual variation of the test conditions the same trend of jet penetration can be observed like in the correlation results of the shadowgraphs.

The structure of the Contour lines for the SMD in Fig. 10 is typical for all test conditions. The form of the contour lines reflects two tendencies: in the vertical direction the influence of inertia leading to bigger droplets away from the nozzle and in the horizontal direction an influence of the dense spray on

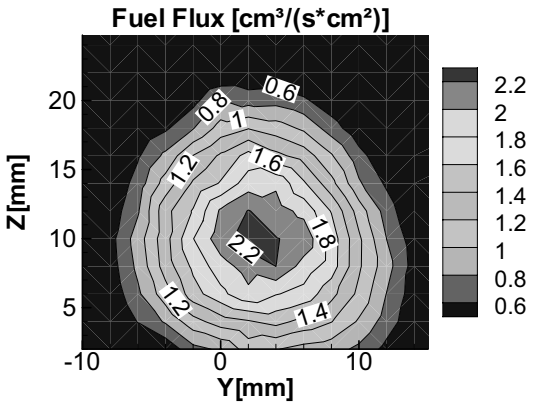

Fig. 9 **Fuel flux recorded at x = 100 mm, p_{air} = 4 bar, u_{air} = 75 m/s, q = 6 and, D = 0.7 mm. The values of fuel flux are scaled.**

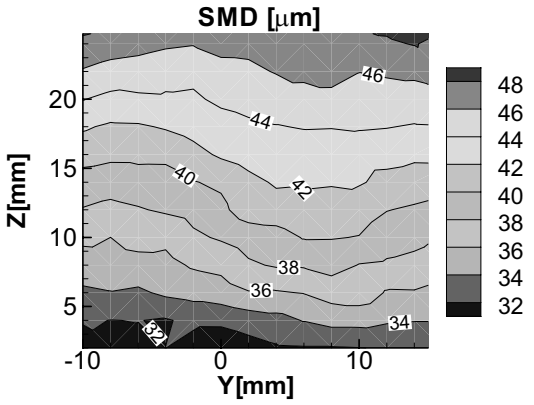

Fig. 10 **SMD data recorded at x = 100 mm, p_{air} = 4 bar, u_{air} = 75 m/s, q = 6 and D = 0.7 mm.**

the atomization and dispersion in the centre of the spray. Here the distance between the droplets might be lower that the turbulence is suppressed and the relative velocity between air and droplets smaller that further atomization is equally suppressed.

A detailed comparison of data for the different test conditions is given in Fig. 11 and in Fig. 12. For this purpose a representative diameter for the global spray was generated according to Ec. (3).

$$SMD_G = \frac{\sum_{i=1}^{n} SMD_i \cdot FuelFlux_i}{\sum_{i=1}^{n} FuelFlux_i} \qquad (3)$$

This form of diameter is a result of local weighting of SMD and fuel flux followed by averaging over the y-z plane. The weighting reflects the fact that droplet sizes are important only at those locations where a non negligible amount of fuel is present.

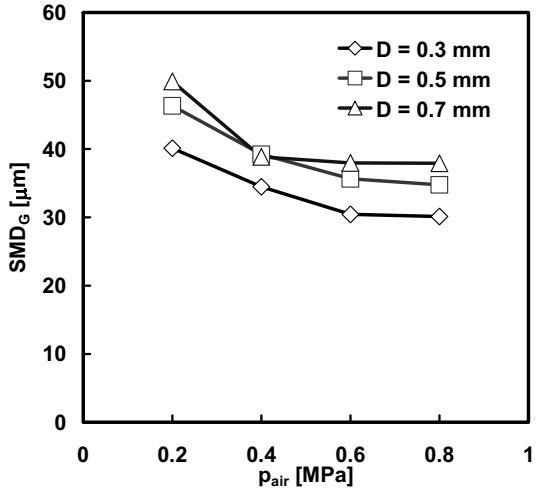

Fig. 11 **Comparison of representative Sauter Mean Diameter of the global spray with the air pressure variation for three nozzle diameters**

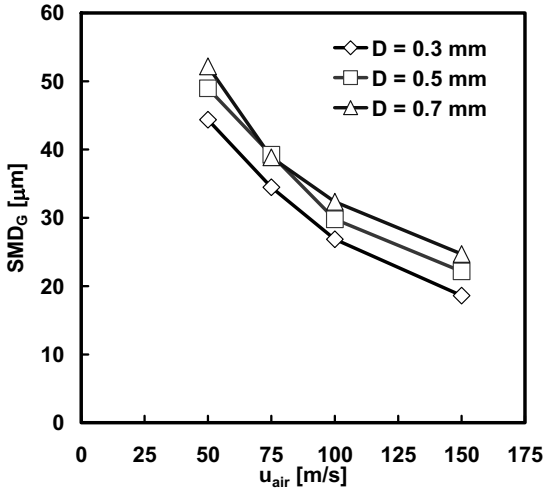

Fig. 12 **Comparison of representative Sauter Mean Diameter of the global spray with the air variation of velocity for three nozzle diameters**

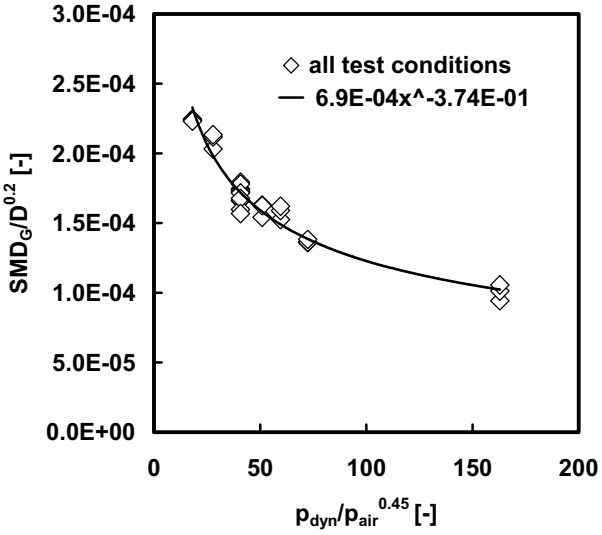

Fig. 13 Correlation of SMD_G

In Fig. 11 it is recognizable a trend to smaller SMD_G with rising pressure for the specific nozzle diameters. For the used range of air velocity this trend to lower droplet size was increased c.p. Fig. 11.

It is apparent that for the smallest nozzle diameter the SMD_G values are likewise smaller. A simple explanation for the diameter influence is the lower surface to volume ratio of bigger diameter jets, which leads to lower surface shear per unit liquid volume.

It can be stated that the influence of momentum flux on SMD_G is marginal and almost negligible. Hence the placement of fuel is decoupled from the fineness of atomization and it is possible to optimize both separately. The independence of SMD from q and therewith from the liquid velocity of the fuel is also observed in other studies [1, 9, 10]. This results from the fact that the air velocity is much higher as the jet velocity, thereby dominating the relative velocity which in turn is decisive for atomization.

Fig. 13 presents the correlation of this data points with a correlation coefficient r = 0.97. Thus for the used operating range, an equation for the Global SMD can be set up like Eq. (4). The applicable values of p_{dyn}, p_{air}, D and SMD_G in SI units relate to the used parameter range, Table 1.

$$SMD_G = 6.9E-04 D^{0.2} \left(\frac{p_{dyn}}{p_{air}^{0.45}} \right)^{-0.374} \qquad (4)$$

SUMMERY

The breakup of a kerosene jet in cross flow was investigated under isothermal conditions. Together with the previous report [1], a comprehensive dataset about a wide range of parameters including the jet diameter is now available.

The data of the current investigation agree well with the previously measured data. The penetration data are very consistent, which is reassuring considering the fact, that the nozzle design was slightly different and considerable differences of the jet behaviour with small design changes have been reported in the literature on automobile injection systems. We attribute this to the fact that neither cavitation nor specifically high pressures were at work. It suggests that the same correlations might be used for sizing the injection system even if the details of the mechanical design are different.

The value of droplet diameters for the used range is primarily depended on pressure and velocity and therefore: the higher the values of pressure and velocity the smaller the droplet diameter. The influence of the liquid momentum flux on the droplet diameter is marginal.

The major influences of the injector hole diameter seem to be the following:

- A higher penetration with bigger hole diameter. The penetration correlation can be conveniently written using the momentum flux density ratio and the distance as dimensionless parameters, but in physical terms it seems that at least for the inspected parameter range, the influence of the hole size on penetration is simply contained in the dependency of the penetration on the liquid momentum flux.
- For the used nozzles it can be stated, that the larger the nozzle the bigger the droplets. This coherence is contained in the generated correlation for the range between 0.3 and 0.7 mm with an exponential dependence of the droplet size on the diameter hole on the order of 0.2.

NOMENCLATURE

Symbol	Quantity	SI Unit
D	hole diameter	m
P	pressure	Pa
q	fuel to air momentum flux ratio	-
SMD	Sauter mean diameter	m
u	velocity component in x direction	m/s
We	Weber number	-

Subscripts

air	air-phase property
dyn	referring to dynamic values
G	flux weighting over a measurement surface

REFERENCES

[1] J. Becker, C. Hassa, “Breakup and Atomization of a Kerosene Jet in Crossflow at elevated Pressure”, Atomization and Sprays, vol. 12, pp. 49-67, 2002

[2] J. Becker, D. Heitz, C. Hassa, “Spray Dispersion in a Counter-Swirling Double-Annular Air Flow at Gas Turbine Conditions“, Atomization and Sprays, vol. 14, pp. 15-35, 2004

[3] C. Hassa, J. Heinze, L. Rackwitz, Th. Doerr, “Validation Methology for the Development of Low Emission Fuel Injectors for Aero-Engines”, ISABE-2005-1143, 2005.

[4] A. Bellofiore, A. Cavaliere, R. Ragucci, “Air Density Effect on the Atomisation of Liquid Jets in Crossflow”, Combustion Science and Technology 179:1, 319 – 342, 2007

[5] T.H. Chen, C. R. Smith, D. G. Schommer, Nejad A.S., „Multi-Zone Behavior of Transverse Liquid Jet in High Speed Flow”, AIAA Paper 93-0453, 1993

[6] M., Brandt, M., Rachner, and G., Schmitz: „An experimental and numerical study of kerosene spray evaporation in a premix duct for gas turbine combustors at high pressure”, Combustion Science and Technology, Vol. 138, pp 313-348, 1998

[7] P. K. Wu, K. A. Kirkendall, R. P. Fuller, “Breakup Processes of liquid jets in subsonic crossflows”, Journal of Propulsion and Power, Vol 13, No 1, pp 64-73, 1997
[8] T. Inamura, N. Nagai, T. Hirai, and H. Asano, “Disintegration Phenomena of Metallized Slurry Fuel Jets in High Speed Air Stream”, Proc. ICLASS-91, Gaithersburg, MD, USA, pp. 839-846, 1991
[9] D. J. Hautmann, T.J. Rosford, “Transverse liquid injection studies”, Technical Paper 90-1965, AIAA, 1990
[10] G.A. Hussein, A.K. Jasuja, R.S. Fletcher, “Penetration and breakup studies of a discrete liquid jet in a cross-flowing air stream – A further study.”, Technical Paper 83-GT-170, ASME, 1983
[11] A. K. Jasuja, “Plain-jet airblast atomization of alternative liquid pretroleum fuels und high ambient pressure conditions”, ASME Paper 82-GT-32, 82